Title
An AAV Dual Vector Strategy Ameliorates the Stargardt Phenotype in Adult Abca4−/− Mice

Journal
Human Gene Therapy, 30(5)

ISSN
2324-8637

Authors
McClements, Michelle E
Barnard, Alun R
Singh, Mandeep S
et al.

Publication Date
2019-05-01

DOI
10.1089/hum.2018.156

Peer reviewed

An AAV Dual Vector Strategy Ameliorates the Stargardt Phenotype in Adult *Abca4*$^{-/-}$ Mice

Michelle E. McClements,[1] Alun R. Barnard,[1] Mandeep S. Singh,[2] Peter Charbel Issa,[1,3] Zhichun Jiang,[4] Roxana A. Radu,[4] and Robert E. MacLaren[1,3,*]

[1]Nuffield Laboratory of Ophthalmology, Nuffield Department of Clinical Neurosciences, University of Oxford, Oxford, United Kingdom; [2]John Hopkins University, Baltimore, MD; [3]Oxford Eye Hospital, Oxford, United Kingdom; [4]Stein Eye Institute, Department of Ophthalmology, David Geffen School of Medicine, University of California at Los Angeles, Los Angeles, California.

The recent approval in the United States of the first adeno-associated viral (AAV) vector for the treatment of an inherited retinal degeneration validates this approach for the treatment of many other diseases. A major limiting factor continues to be the size restriction of the AAV transgene at under 5 kb. Stargardt disease is the most prevalent form of recessively inherited blindness and is caused by mutations in *ABCA4*, the gene that codes for ATP-binding cassette transporter protein family member 4, which has a coding sequence length of 6.8 kb. Dual vector approaches increase the capacity of AAV gene therapy, but at the cost of substantially reduced levels of target protein, which may be insufficient to achieve a therapeutic effect. Here we show that the efficacy of recombination of dual vectors is dependent on the length of DNA overlap between two transgenes. With optimized recombination, full-length ABCA4 protein is expressed in the photoreceptor outer segments of *Abca4*$^{-/-}$ mice at levels sufficient to reduce bisretinoid formation and correct the autofluorescent phenotype. These observations support a dual vector approach in future clinical trials using AAV gene therapy to treat Stargardt disease.

Keywords: adeno-associated virus, gene therapy, dual vector, ABCA4, Stargardt disease

INTRODUCTION

ADENO-ASSOCIATED VIRUS (AAV) is the current vector of choice for retinal gene therapy due to its ability to diffuse through the various cell layers within the retinal structure, low immunogenicity, excellent tropism for photoreceptor cells, and extensive proof of concept in a variety of preclinical models.[1] Human clinical trials have shown safety and efficacy with AAV vectors in the retina and gene therapy trials for multiple conditions have been reported.[2–7] For some disorders, such as Stargardt disease, the therapeutic genes are too large to fit within a transgene that can be packaged into a single AAV capsid. Gene supplementation therapy for these disorders is therefore an intriguing challenge. Given the restricted packaging capacity of AAV, its potential to treat "large gene" diseases initially seemed limited, yet in the past decade, studies have indicated that AAV delivery of genes over 3.5 kb in size using two or more AAV particles is a distinct possibility.[8–17] Through systematic design variations of an overlapping dual vector system, (Fig. 1) we achieved therapeutic levels of ATP-binding cassette transporter protein family member 4 (ABCA4) and reduced the production of truncated protein forms that are a known side effect of dual vector strategies.[10,12,14]

Stargardt disease resulting from mutations in the *ABCA4* gene is the most commonly inherited macular dystrophy and often becomes symptomatic in childhood but after the period of visual development, which provides ample opportunity for therapeutic intervention to prevent or slow further sight loss.[18] Lack of functional ABCA4 prevents the transport of free retinaldehyde from the luminal to the cytoplasmic side of the photoreceptor cell disc outer membranes, resulting in increased formation of retinoid dimers (bisretinoids). Upon daily

*Correspondence: Prof. Robert E. MacLaren, Nuffield Laboratory of Ophthalmology, Nuffield Department of Clinical Neurosciences, Levels 5 & 6 West Wing, The John Radcliffe Hospital, Headley Way, Oxford OX3 9DU, United Kingdom. E-mail: enquiries@eye.ox.ac.uk

DOI: 10.1089/hum.2018.156

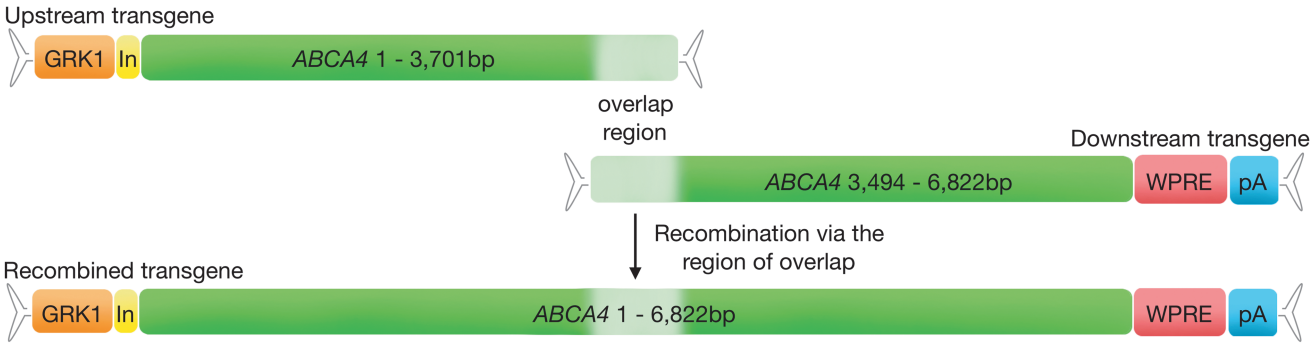

Figure 1. Outline of the *ABCA4* overlapping dual vector system. The elements of an adeno-associated virus (AAV) transgene were split across two independent transgenes (upstream and downstream). The upstream transgene contained the promoter and upstream fragment of *ABCA4* coding sequence, and the downstream transgene carried a downstream fragment of *ABCA4* coding sequence plus a WPRE and pA. Once inside the same host cell nucleus, the two transgenes align and recombine via the region of overlap. ABCA4, human ATP-binding cassette transporter protein family member 4; GRK1, human rhodopsin kinase promoter; In, intron; pA, polyA signal; WPRE, Woodchuck hepatitis virus posttranscriptional regulatory element.

phagocytosis of photoreceptor outer segments by the retinal pigment epithelium (RPE), the retinoid derivatives are processed but are insoluble and accumulate.[19] This leads to dysfunction and eventual death of the RPE cells with subsequent secondary loss of the overlying photoreceptors. We have previously characterized the fundus changes in the pigmented *Abca4*$^{-/-}$ mouse model[20] and documented the positive effects of deuterized vitamin A on fundus fluorescence and bisretinoid accumulation.[21] Here we show for the first time that gene supplementation of *ABCA4* in the photoreceptors of the *Abca4*$^{-/-}$ mouse model using an overlapping AAV dual vector system reduces the buildup of toxic bisretinoids. Such an effect in a patient with Stargardt disease could prevent death of the RPE cells and the photoreceptor cells they support.

MATERIALS AND METHODS

Vector design

NM_000350 was used with the exception of the following nucleotide changes that did not influence the amino acid sequence: 1,536 G>T; 5,175 G>A; 6,069 T>C. Codon optimization of this *ABCA4* coding sequence was performed and generated by GenScript (Piscataway, NJ). Full-length *ABCA4* coding sequence (6,822 nucleotides) was inserted into plasmids to generate CAG.ABCA4.pA and CAG.coABCA4.pA. Upstream transgenes for *in vitro* comparisons contained the CMV.CBA enhancer/promoter elements prior to an *ABCA4* coding sequence fragment (Table 1) generated by PCR before cloning in between AAV2 inverted terminal repeats (ITRs) via SwaI restriction sites. Upstream transgenes for *in vivo* experiments contained the human rhodopsin kinase (*GRK1*) promoter.[22] For the optimized upstream transgene, 176 nucleotides of the CAG intron region were amplified and attached to the end of the *GRK1* promoter by PCR. Downstream transgenes were identical for *in vitro* and *in vivo* use, the desired fragments of *ABCA4* coding sequence (Table 1) were amplified and attached to woodchuck hepatitis virus post-transcriptional regulatory element and bovine growth hormone polyA signal by PCR before being inserted into ITR containing plasmids. Numerous primers were used for vector creation and primer designs are available on request.

AAV production

HEK293T cells were grown in HYPERFlasks (SLS, UK) and transfected using a typical PEI protocol to deliver a total of 500 μg of the required plasmids: pRepCap, pHelper (pDeltaAdF6) and pTransgene. Cells were harvested 3 days after transfection, lysed, and the AAV population isolated by ultracentrifugation with an iodixanol gradient followed by purification in Amicon Ultra-15 100K filter units (MerckMillipore, UK). The

Table 1. *Details for the dual vector combinations tested*

Overlapping dual vector name	*Upstream vector*		*Downstream vector*		*Overlap length*	*Overlap GC content*
	Transgene length	ABCA4 *CDS*	*Transgene length*	ABCA4 *CDS*		
A	4.9kb	1–4,326	4.9kb	3,154–6,822	1,173bp	55%
B	4.3kb	1–3,701	4.8kb	3,196–6,822	505bp	54%
C	4.3kb	1–3,701	4.6kb	3,494–6,822	207bp	52%
D	4.3kb	1–3,701	4.5kb	3,603–6,822	98bp	48%
E	4.3kb	1–3,701	4.4kb	3,653–6,822	48bp	47%
F	4.3kb	1–3,701	4.4kb	3,678–6,822	23bp	38%
X	4.3kb	1–3,701	4.3kb	3,701–6,822	0bp	N/A
InC	4.3kb	1–3,701	4.6kb	3,494–6,822	207bp	52%

ABCA4, ATP-binding cassette transporter protein family member 4; bp, base pairs; CDS, coding sequence; N/A, not applicable.

final preparations were collected in phosphate-buffered saline (PBS). SDS-PAGE analysis was used to confirm good purification of each preparation and qPCR titers were determined using primers targeting either the upstream (forward [FW] 5′GCACCTTGGCCGTATTTGGACAG; reverse [RV] 5′TGAGTCAGACAGGCCGATGT) or downstream (FW 5′TGGCGCAGATCGTGCT; RV 5′ACAGAAGGAGTCTTCCA) portion of *ABCA4* coding sequence. Primer sets were confirmed to have 95–105% efficiency.

In vitro experiments

All *in vitro* experiments were performed with HEK293T cells, which were passaged using standard protocols and transfected at 60–70% confluence with equal molarities of plasmid using the *Trans*IT-LT1 transfection reagent (Mirus Bio). Cells were incubated for 48 hours at 37°C with 5% CO_2 after which the media was removed and the cells were washed in cold PBS before collecting the cell pellets. For transductions, each AAV was applied at a mulitiplicity of infection of 20,000 in a half well volume of media without FBS and with 200 nM doxorubicin (Sigma-Aldrich, UK) and incubated at 37°C, 5% CO_2 for 1 hour. The remaining volume of media was then added to each well containing 20% FBS and cells were incubated at 37°C, 5% CO_2 with a media change conducted 2 and 4 days after transduction. Cells were harvested 1 week after transduction.

In vivo experiments

All animal breeding and experimental procedures were performed under approval of local and national ethical and legal authorities and were conducted in compliance with the Association for Research in Vision and Ophthalmology statement for the use of animals in ophthalmic and vision research. Pigmented *Abca4*$^{-/-}$ mice (129S4/SvJae-*Abca*^{4tm1Ght}) were provided by Gabriel Travis (David Geffen School of Medicine, University of California, Los Angeles, CA) and bred in the Biomedical Sciences Division, University of Oxford. Pigmented wild-type control mice (129S2/SvHsd) were purchased from ENVIGO (Hillcrest, UK). Animals were kept in a 12-hour light (<100 lux)/dark cycle with food and water available *ad libitum*. Subretinal injections were performed at 4–5 weeks of age by delivering 1–2 μL of reagent under direct visual guidance using an operating microscope (Leica Microsystems, Germany). Assessments in Supplementary Fig. S1 used a scleral tunnel approach through the posterior pole to the superior retina with a Hamilton syringe and 34-gauge needle (ESS labs, UK). All other subretinal injections involved an anterior chamber paracentesis with a 33G needle prior to subretinal injection using a WPI syringe and beveled 35-gauge needle system (World Precision Instruments, UK). Animals were anesthetized by intraperitoneal injection containing ketamine (80 mg/kg) and xylazine (10 mg/kg) and pupils fully dilated with tropicamide and phenylephrine eye drops (Bausch & Lomb, UK). Proxymetacaine eye drops (Bausch & Lomb, UK) were applied prior to subretinal injection. Post-injection, chloramphenicol eye drops were applied (Bausch & Lomb) and anesthesia was reversed with atipamezole (2 mg/kg) and carbomer gel applied (Novartis, UK).

In vivo imaging and analysis

Mouse fundus autofluorescence imaging using a confocal scanning laser ophthalmology (SpectralisHRA, Heidelberg Engineering, Heidelberg, Germany) was performed using a standardized protocol based on previously described methods.[20,23] Animals were anesthetized and pupils fully dilated as detailed above. A custom-made contact lens was placed on the cornea with hypromellose eye drops (Alcon, UK) as a viscous coupling fluid. The NIR reflectance image (820 nm diode laser) was used to align the fundus camera relative to the pupil and to focus on the highest reflectivity in the outer retina. Fluorescence was excited using a 790 nm diode laser. Images were recorded using the "automatic real time" mode, set to average 24 consecutive. The mean grey value of autofluorescence images were extracted by measuring a standardized ring shaped area at the inferior retina between 250 and 500 pixel radii from the optic disc center using ImageJ software (Supplementary Fig. S2).

Transcript analysis

Messenger RNA was extracted using mRNA DIRECT Dynabeads-oligodT (Life Technologies, UK) with 500ng used in SuperScript III cDNA synthesis reaction with oligodT primer. The cDNA was cleaned in QIAGEN spin columns and eluted in 50 μL water. Quantitative PCRs used 2 μL of each cDNA preparation (primers above), *ABCA4* levels were normalized to *ACTIN*/*Actin*. In RT-PCRs, 2 μL of cDNA was used for overlap (FW 5′ACCTTGATCAGGTGTTTCCA, RV 5′ACAGAAGGAGTCTTCCA) and 5′UTR assessments (FW 5′CCACTCCTAAGCGTCCTC, RV 5′CAGGGATTGTTCACATTGC). Amplicons for sequence analysis were PCR purified or cloned and purified before Sanger sequencing.

Western blot assessment

Samples were lysed in RIPA buffer (MerckMillipore, UK) plus proteasome inhibitor (Roche, UK) and 10% glycerol using a hand-held homogenizer prior to centrifugation. Supernatants were removed and 20 μL added to 5 μL protein loading buffer (GeneFlow, UK). Samples were run on a 7.5% Tris-Glycine gel (TGX, BioRad, UK) and transferred to a polyvinylidene difluoride membrane using a TransBlotTurbo. ABCA4/Abca4 (ab72955, Abcam, UK; Supplementary Fig. S3C) and GAPDH/Gapdh detection (TA802519, Origene) was conducted using a SNAPiD system (MerckMillipore, UK). Blots in Supplementary Fig. S1 used horseradish peroxidase (HRP)-conjugated secondary antibodies (Abcam, UK) developed with Luminata Forte HRP substrate (MerckMillipore, UK). All other blots used IRDye fluorescent secondary antibodies (LI-COR Biosciences, UK). Signals were recorded with the Odyssey imaging system and band densities assessed using Image Studio Lite software. ABCA4/Abca4 levels were normalized to GAPDH/Gapdh levels and values presented relative to background readings of negative control samples.

Immunohistochemistry

Following enucleation, the lens and cornea were removed and each eye cup incubated in 4% paraformaldehyde and passed through sucrose solution before being frozen in O.C.T compound (VWR, UK). Eyes were sectioned and dried before permeabilizing with 0.2% Triton-X 100. Slides were washed in PBS before blocking with 10% bovine serum albumin (BSA), 10% serum. Slides were washed prior to primary antibody incubation (1/200 in 1% BSA, 1% serum) and secondary antibody incubation (1/400 in 1% BSA, 1% serum). Hoescht stain was performed (Sigma-Aldrich,UK) (1/1,000 in PBS) prior to a final wash. ProLong Diamond antifade mounting medium (ThermoFisher, UK) was applied and slides sealed before imaging. Primary antibodies were: ABCA4 (goat polyclonal, ABIN343052, AntibodiesOnline, Germany; Supplementary Fig. S3C) and Hcn1 (mouse monoclonal, ab84816, Abcam, UK). Secondary antibodies were donkey Alexa Fluor: anti-goat 488 (ab1050129, Abcam, UK) and anti-mouse 568 (ab175472, Abcam, UK).

High-performance liquid chromatography analysis of bisretinoid content

These assessments were performed with the identity of each eye masked. Enucleation was conducted under dim red light and eyes were immediately frozen and stored at –80°C, protected from light, and then shipped frozen to the Jules Stein Eye Institute. Bisretinoid extraction and assessment by high-performance liquid chromatography (HPLC) was performed on the eyes as previously described.[24] The identity of each sample was only revealed once all eyes had undergone HPLC assessment and paired eyes could then be compared.

Statistical analysis

Each data set was assessed for normal distribution (Shapiro–Wilk test) and variance (Brown–Forsythe test). If data for comparison were skewed and unpaired then nonparametric tests were performed (Mann–Whitney *U*-test or Kruskal–Wallis). If the data were normally distributed and paired, then parametric tests were used (Student's *t*-test or ANOVA). Multiple comparisons were conducted with correction using either Tukey's or Sidak's comparisons test (if ANOVA) or Dunn's comparisons (if Kruskal–Wallis). Figure legends indicate the test used to analyze each specific data set with n, p, and F values provided where appropriate. Data are shown as mean and standard error of the mean.

RESULTS

Capsid and coding sequence selections

Initial comparisons of ABCA4 protein levels were compared from wild-type and codon-optimized *ABCA4* coding sequences tested in HEK293T cells (Supplementary Fig. S1A) and *Abca4*$^{-/-}$ mice (Supplementary Fig. S1B). Whilst ABCA4 detection was higher when using a codon-optimized construct in plasmid form, for dual vector AAV recombination it was found that use of the wild-type sequence *in vivo* was more efficacious (Supplementary Fig. S1B). It should be noted that changing codons also affects DNA base pairing and hence has a direct influence on dual vector recombination in this scenario.

Changes to the AAV capsid protein amino acids by substituting tyrosine (Y) for phenylalanine (F) have been shown to improve transduction in wild-type mice[25] and in the *Abca4*$^{-/-}$ retina.[26] We therefore compared the success of the overlapping dual vector approach in *Abca4*$^{-/-}$ retinae using identical transgenes packaged in either AAV8 or AAV8 Y733F capsids; 31.3 ± 7.8 times more *ABCA4* transcripts were detected in *Abca4*$^{-/-}$ retinae injected with the AAV8 Y733F dual vectors ($p = 0.0002$, Supplementary Fig. S1C). We therefore continued our investigations using the AAV8 Y733F capsid.

Comparisons of different overlapping regions

Six overlap variants were prepared (A–F), ranging from the maximum possible length (1,173 bp) to a minimum consistent with maintaining specificity

(23 bp). An additional variant (X) designed with no overlapping region between transgenes acted as a negative control (Table 1). Overlap variants B–X shared the same upstream transgene and differed only in the *ABCA4* coding sequence contained in their downstream transgene. An extension of the upstream transgene was required to obtain the maximal 1,173 bp overlap zone for variant A.

HEK293T cells were transduced with each overlapping variant and ABCA4 expression measured by Western blot. The overlap region was observed to have a significant influence on the levels of ABCA4 generated ($p < 0.0001$, Fig. 2). These dual vector variants were injected into the subretinal space of *Abca4*$^{-/-}$ mice and the neural retinae removed for ABCA4 detection. Full-length ABCA4 production was evident by Western blot with dual vector variants A–F (Supplementary Fig. S3A).

Including an intron immediately after the promoter has been shown to augment gene expression[27] and in a dual vector context, including an intron had a significant influence on levels of full-length ABCA4 achieved, with a minimum 1.5-fold increase in detection observed following treatment with overlapping variants ($p = 0.004$, Supplementary Fig. S3B). Subsequent injections with the optimized dual vector variant InC enabled consistent detection of full length ABCA4 in *Abca4*$^{-/-}$ injected eyes (Fig. 2C).

Sequencing across the overlap zones confirmed that *ABCA4* transcripts generated from recombined transgenes did not carry mutations (Supplementary Fig. S4A) and the intron was confirmed to be successfully spliced from mRNA transcripts (Supplementary Fig. S4B). Hence the dual vector system had been optimized in terms of capsid, overlap zone and transgene regulatory elements.

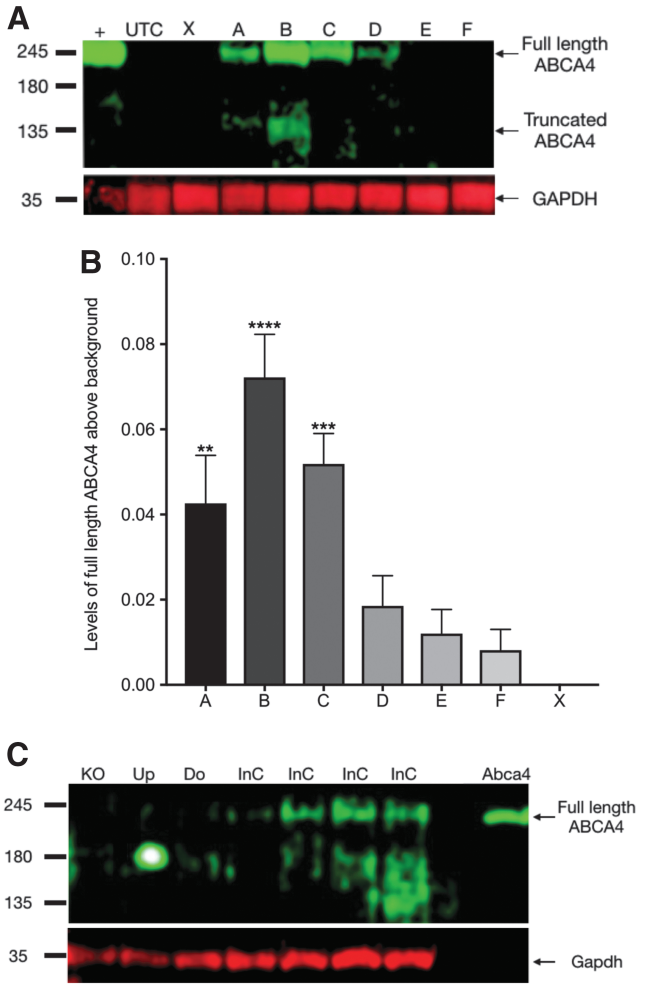

Figure 2. Assessment of overlapping upstream and downstream AAV8 Y733F ABCA4 dual vectors. **(A)** Transduced HEK293T cells generated full length ABCA4. **(B)** A significant influence of the overlapping region on the levels of ABCA4 was identified *in vitro* (one-way ANOVA, $n = 6$, $p < 0.0001$, $F(6,35) = 12.81$). Variants A, B, and C generated significantly more ABCA4 than variant X (one-way ANOVA, Tukey's multiple comparisons test; A, $^{**}p = 0.004$; B, $^{****}p < 0.0001$; C, $^{***}p \leq 0.0004$). Error bars represent SEM. **(C)** Dual vector overlap variant InC was injected into *Abca4*$^{-/-}$ mouse eyes with consistent detection of full length ABCA4 achieved 6 weeks postinjection (one eye per lane). +, HEK293T cells transfected with pCAG.ABCA4; Abca4, mouse ATP-binding cassette transporter protein family member 4 (positive control); Do, *Abca4*$^{-/-}$ eye injected with downstream vector; GAPDH, glyceraldehyde 3-phosphate dehydrogenase; InC, optimized dual vector system; KO, uninjected *Abca4*$^{-/-}$; Up, *Abca4*$^{-/-}$ eye injected with upstream vector; UTC, untransduced HEK293T cells.

Limiting production of truncated ABCA4

A key aspect in the optimization of the dual vector system was limiting unwanted expression from unrecombined transgenes. Despite detection of *ABCA4* mRNA transcripts from upstream vector only injected eyes, absence of truncated ABCA4 protein forms was confirmed with constructs containing an N-terminus FLAG tag (Supplementary Fig. S5). However, C-terminus protein detection identified truncated ABCA4 protein ~135 kDa following dual and downstream vector-only treatment (Figs. 2 and 3). Expression from unrecombined downstream transgenes was anticipated to result from the native promoter activity of the AAV2 ITR.[28] The *ABCA4* coding sequence contained in the downstream transgenes significantly influenced the levels of truncated ABCA4 detected with only A and B unrecombined downstream constructs generating consistently detectable truncated ABCA4 ($p = 0.0003$, Fig. 3). In a dual vector context, variants A–D generated clearly detectable ABCA4 forms (Fig. 2A), and of the total ABCA4 population, cells treated with variants A and B achieved a truncated ABCA4 proportion of $21 \pm 5\%$ and $25 \pm 1\%$, respectively, whereas variant C and D treated samples were $4 \pm 2\%$ and $3 \pm 3\%$, respectively. Downstream con-

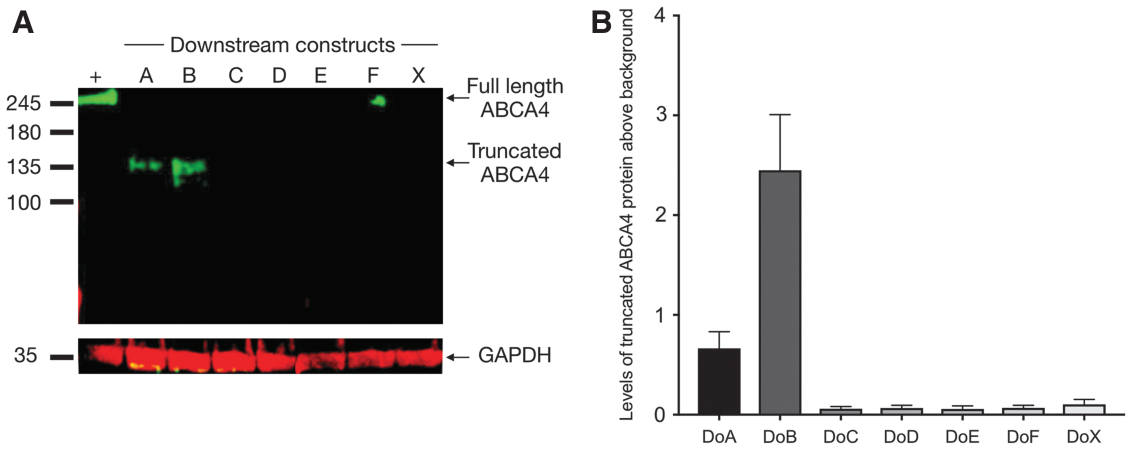

Figure 3. **(A)** HEK293T cells transfected with downstream transgene constructs revealed that generation of truncated ABCA4 was only detectable from downstream variants A and B. **(B)** Levels of truncated ABCA4 generated from Unrecombined downstream transgenes was significantly influenced by the transgene variant (Kruskal–Wallis, $n=6$, $p=0.0003$). Error bars represent SEM. +, HEK293T cells transfected with pCAG.ABCA4.

structs A and B contained in-frame ATG codons prior to any out-of-frame codons, whereas variants C–X contained out-of-frame ATG codons prior to any in-frame ATG codons downstream of the 5′ITR.

Taking into consideration the desire to reduce expression of truncated ABCA4 from the downstream vector, a compromise was made to select overlap C (207 bp), which although slightly less efficient than B (505 bp), gave a purer ABCA4 protein population, which would have safety benefits in the clinical scenario. Therefore, overlap C downstream vector was combined with the intron-containing upstream vector. This optimal dual vector combination (InC) was used for subsequent testing in the *Abca4*$^{-/-}$ mouse at 1×10^{10} genome copies per vector, per eye.

Confirmation of ABCA4 expression in photoreceptor cells

ABCA4 is a large, complex, folded protein that undergoes post-translational modifications and is trafficked to the cell membrane of the specialized photoreceptor outer segments. Immunohistochemical localization of ABCA4 therefore provides indirect information on protein structure after dual vector transduction by subretinal injection. Anti-Hcn1 was used to highlight the limit of the photoreceptor inner segments. Uninjected *Abca4*$^{-/-}$ eyes and those that received a sub-retinal injection of either upstream or downstream vector-only exhibited no detectable ABCA4 staining (Fig. 4B, C, and D, respectively). The absence of staining in downstream vector-only injected eyes aligned with the reduction of truncated ABCA4 observed by Western blot (Fig. 3). Importantly, truncated ABCA4 from unrecombined downstream transgenes would generate a nonspecific expression pattern given the absence of a cell-specific promoter, yet we observed no truncated ABCA4 staining up to 6 months after injection (Supplementary Fig. S6A). For *Abca4*$^{-/-}$ eyes injected with the optimized dual vector system, ABCA4 staining was evident in the outer segments of photoreceptor cells (Fig. 4E) with expression detected up to 6 months after injection (Supplementary Fig. S6B). The area of ABCA4 staining in a dual vector injected eye was observed to extend from the site of injection in the superior retina into the inferior retina (Supplementary Fig. S6C).

Reduction in buildup of toxic bisretinoids

The accumulation of bisretinoids is the hallmark of Stargardt disease and is believed to be the major driver for retinal degeneration in humans. This study used pigmented *Abca4*$^{-/-}$, a mouse model without significantly abnormal photoreceptor cell loss.[20] However, a consistent feature of these mice is the extensive accumulation of quantifiable bisretinoids over time, thus recapitulating a key pathological hallmark of the human disease.[20,23,29]

In a blinded study, eyes of 13 *Abca4*$^{-/-}$ mice received the upstream vector-only in one eye (sham) and the dual vector in the contralateral eye (treatment), with each eye receiving the same total AAV dose. Eyes were harvested in dark conditions, processed, and analyzed by high performance liquid chromatography to determine levels of all-*trans*-retinal dimer-phosphatidylethanolamine, *N*-retinylidene-*N*-retinylphosphatidylethanolamine (A2PE), di-hydro-A2PE, and conjugated *N*-retinylidene-*N*-retinylphosphatidylethanolamine (A2E) and its major *cis*-isomer (iso-A2E). Data are presented as a

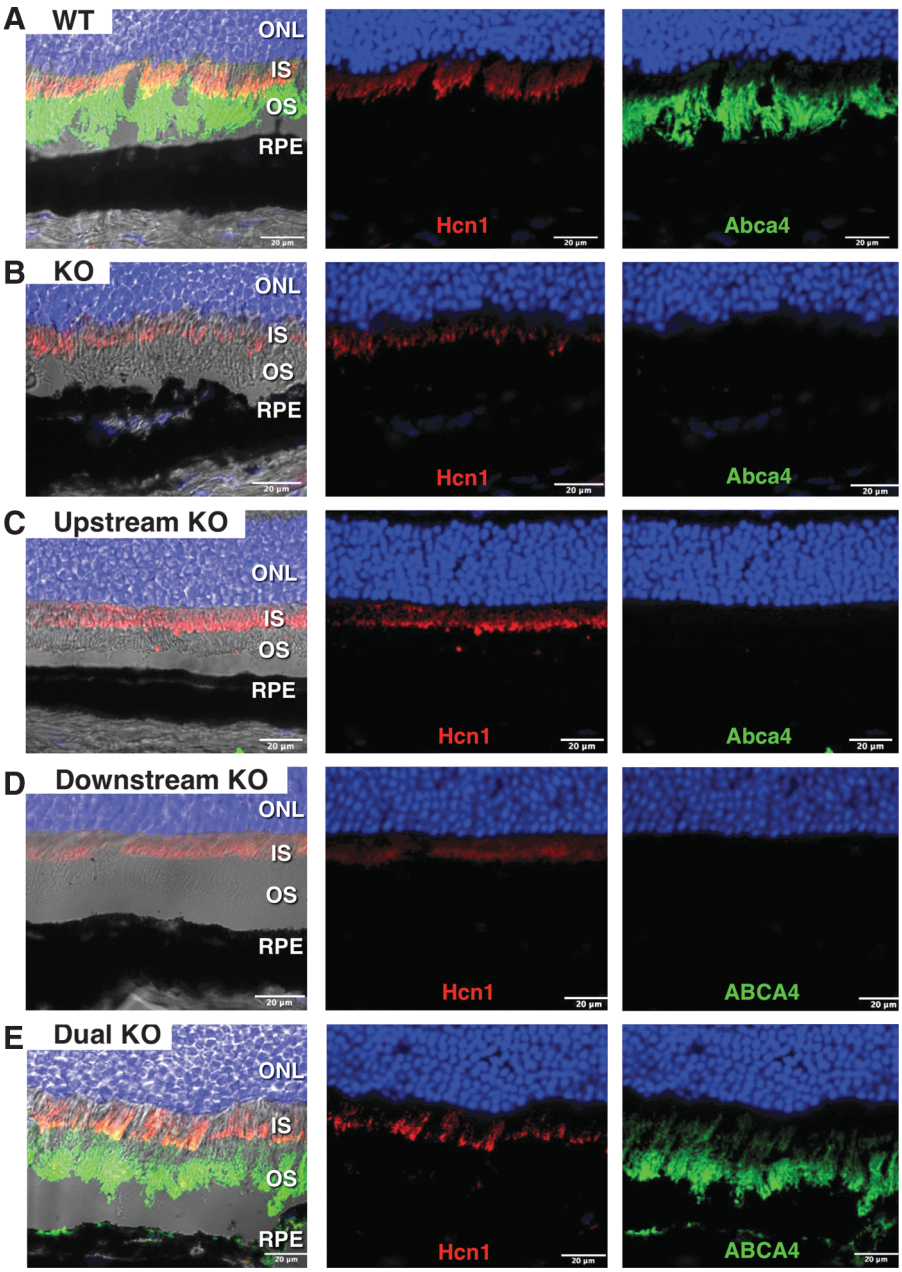

Figure 4. Sections of mouse eyes stained for ABCA4 (green) and Hcn1 (red). Nuclei were stained with Hoescht. **(A)** Abca4 staining in photoreceptor outer segments of WT SVEV 129. **(B)** Absence of Abca4 staining in uninjected *Abca4*$^{-/-}$ **(C)** Absence of ABCA4 in upstream vector injected *Abca4*$^{-/-}$. **(D)** Absence of ABCA4 staining in downstream vector injected *Abca4*$^{-/-}$. **(E)** ABCA4 staining in photoreceptor outer segments of dual vector injected *Abca4*$^{-/-}$. Dual, dual vector injected; Downstream, downstream vector injected; Hcn1, hyperpolarization activated cyclic nucleotide gated potassium channel 1 (inner segment marker); IS, inner segments; ONL, outer nuclear layer; OS, outer segments; RPE, retinal pigment epithelium; Upstream, upstream vector injected *Abca4*$^{-/-}$; WT, SVEV wild type.

comparison of the levels of each biomarker in paired eyes. The treatment was observed to have a significant influence on the bisretinoid levels in *Abca4*$^{-/-}$ mouse eyes compared to sham injected eyes ($p = 0.03$, Fig. 5B). This is the first presentation of a dual vector treatment for Stargardt disease affecting the biochemistry of the *Abca4*$^{-/-}$ mouse model and thus inducing a positive therapeutic effect.

Reduction in 790 nm fundus autofluorescence

Directly measuring bisretinoid levels in *Abca4*$^{-/-}$ mice enabled quantifiable assessment of therapeutic efficacy. However, looking towards a human clinical trial endpoint, scanning laser ophthalmoscopy (SLO) assessment of autofluorescence was also performed using the 790 nm wavelength as an *in vivo* measure for melanolipofuscin accumulation.[20] In this cohort, mice received a sham injec-

tion of PBS to control for the effects of retinal detachment, whilst the contralateral eye received the optimized overlapping dual vector system. A standardized SLO protocol based on previous work was used,[30] and when extracting the mean grey value of each image, a standardized area of measurement was taken only from the inferior retina near the optic nerve to avoid disrupted autofluorescence caused by surgically induced changes around the site of injection which was in the superior hemiretina (Supplementary Fig. S2). Between 3 and 6 months postinjection, the increase in levels of 790 nm autofluorescence was significantly attenuated in the ABCA4 dual vector injected eyes compared with the paired sham injected eyes ($p = 0.04$, Fig. 5D).

DISCUSSION

Since AAV-mediated gene therapy has now become an approved treatment for inherited retinal degeneration, the ability to increase the size of the AAV transgene would widen the therapeutic indications considerably. Here we focus on recessive *ABCA4* mutations which are responsible for Stargardt disease and other cone and cone–rod dystrophies.[31] The size of the *ABCA4* coding sequence allowed us to explore different degrees of overlap in order to identify a critical zone for optimal dual vector recombination. Previously, questions have been raised regarding whether these strategies could lead to production of enough target protein to provide therapeutic effect. In the Stargardt mouse

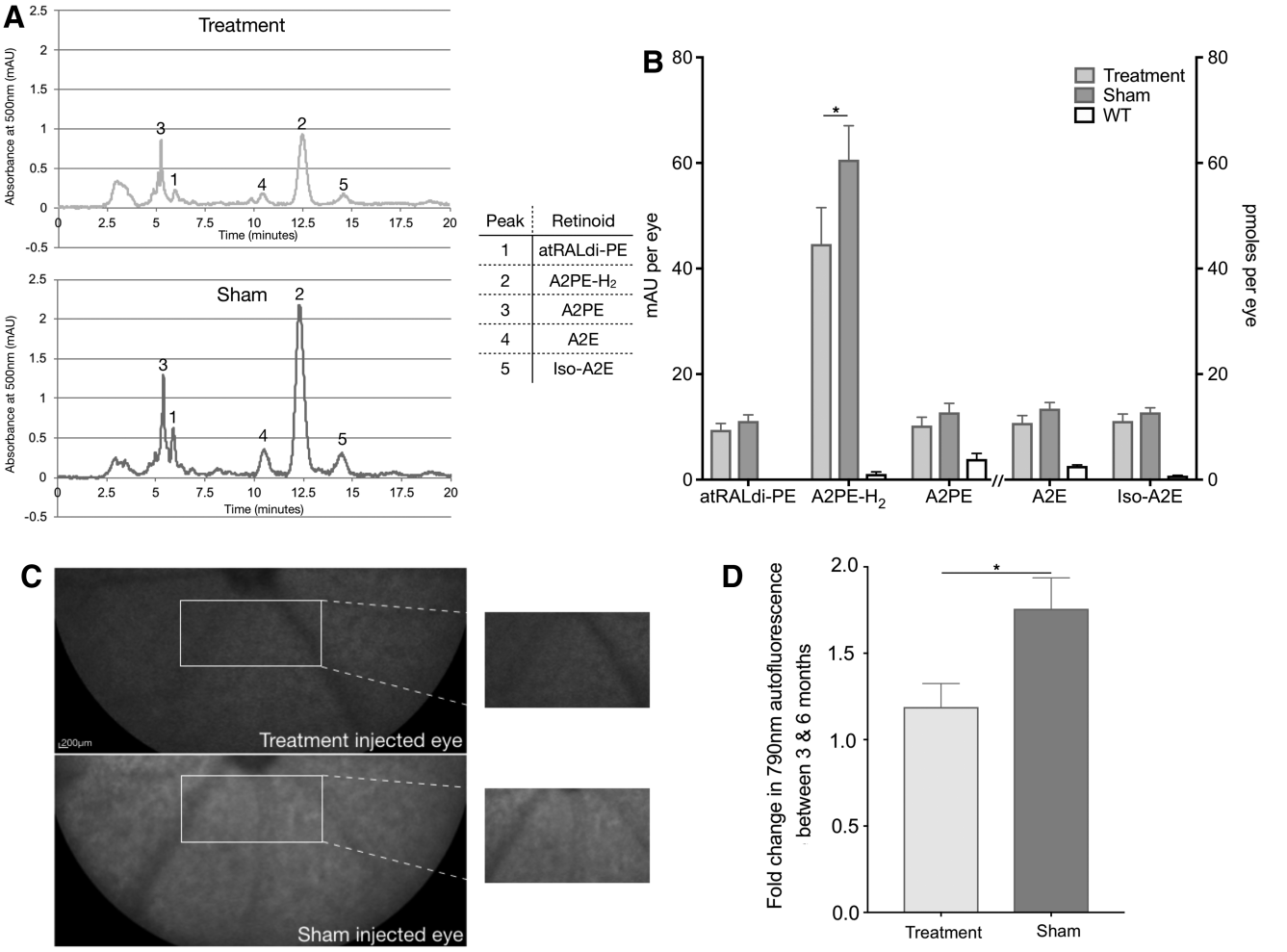

Figure 5. Dual vector therapeutic effects in the *Abca4*$^{-/-}$ mouse model. **(A)** Representative chromatogram traces for treatment and sham injected eyes. **(B)** A significant reduction in bisretinoid levels was observed in eyes that received the dual vector treatment compared to paired sham injected eyes (two-way ANOVA with matching values, n = 13, treatment effect p = 0.03, F(1,60) = 4.516). A multiple comparisons test identified a significant difference in A2PE-H_2 levels between treatment and sham injected eyes (*p = 0.01). Bisretinoid levels in WT eyes are presented for reference only and were not included in the analysis. **(C)** Paired treated and sham injected *Abca4*$^{-/-}$ eyes were imaged by scanning laser ophthalmology (SLO). **(D)** Between 3 and 6 months postinjection, the increase in 790nm autofluorescence was significantly attenuated in eyes that received dual vector (treatment) compared to paired sham-injected eyes (paired *t*-test, $n = 12$, $^*p = 0.04$). atRALdi-PE, all-trans-retinal dimer-phosphatidylethanolamine; A2PE-H_2, di-hydro-A2PE; A2PE, N-retinylidene-N-retinylphosphatidylethanolamine; A2E, conjugated N-retinylidene-N-reintylphosphatidylethanolamine; iso-A2E, isomer of A2E; WT, SVEV age-matched controls.

model, therapeutic effect can be readily assessed as the target protein, ABCA4, is required in abundance in the photoreceptor cells of the retina and its absence induces the accumulation of bisretinoid compounds, which in turn leads to an increase in autofluorescence. The therapeutic potential of the overlapping dual vector system was validated by observing a reduction in this bisretinoid accumulation and fundus autofluorescence levels following treatment.

The most critical aspect of an overlapping dual vector strategy is the event of recombination between two transgenes. Six different overlap regions ranging from 23 to 1,173 bp were compared, with the best performing being 207–505 bp. A recent report compared 0.3 kb, 0.6 kb, and 1.0 kb overlap regions of a *lacZ* gene in an overlapping dual vector system and identified the largest overlap region as being the most efficient.[11] However, in another report, a 0.07 kb F1 phage-derived sequence has proven to be efficient for achieving recombination between hybrid dual vectors in photoreceptor cells.[14] There are currently no clearly defined characteristics of what makes a region efficient at recombination. While a longer region of overlap may seem logical to increase the opportunity for intermolecular interactions, it may also be less available for such interactions due to secondary structure formation, whereas shorter overlaps might be problematic in the strength of their binding to the opposing transgene molecule. This study highlights the importance of assessing multiple overlapping regions to determine the optimal sequence for a given dual vector system.

Critical to assessing the safety of a dual vector system is the identification of unwanted by-products from unrecombined transgenes. Testing of upstream or downstream vectors (not in combination) revealed that each vector was capable of generating truncated *ABCA4* mRNA transcripts. The upstream transgene nucleotide sequence contained a SwaI restriction site used for cloning purposes that was suspected to be acting as a cryptic polyA signal: TTTAAA, which has been identified as a polyA signal in 1–2% of human genes.[32,33] The absence of any protein detection following treatment with the upstream vector could be attributed to the lack of an in-frame stop codon in the resulting mRNA transcript, which would lead to degradation of any generated peptide.[34] Given the overexpression achieved when testing our upstream transgenes and that other publications using an N-terminus FLAG-tag with ABCA4 have detected truncated protein forms,[14] we believe our inability to detect truncated protein from the upstream transgene to be genuine. Truncated ABCA4 protein was detected from original downstream vector designs (Fig. 3). Other research groups have attempted to reduce unwanted protein production from dual vectors by inclusion of additional genetic sequences in the transgene design.[14] However, our own attempts employed sequence selection of coding regions that carried out-of-frame ATG codons prior to any in-frame ATG codons within 100 bases of the 5′ITR, reducing truncated ABCA4 to negligible levels (Fig. 3). This sequence design was based on evidence that ribosomes favor initiating translation from the first AUG codon they encounter in good context.[35,36] Translation from unrecombined downstream transgenes at an out-of-frame AUG would generate only short peptides before an out-of-frame stop codon was reached, such short peptides would then be degraded by the cell due to their size.[37,38]

Studies have shown that mRNA transcripts which undergo splicing may exhibit higher translational yields than equivalent intronless transcripts and placing the intron near the promoter enhances gene expression more than when used inside the coding sequence.[24,39] Our data reinforce these previous findings, supporting the standard use of introns in vector transgenes.

Other dual vector approaches[14,15,16] and nanoparticle delivery[40] led to successful ABCA4 expression in adult *Abca4*$^{-/-}$ mice and provided evidence of positive effects attributed to ABCA4 expression. In this study, we have, for the first time, shown convincing expression of ABCA4 in the photoreceptor outer segments of adult *Abca4*$^{-/-}$ mouse retinae following injection with an overlapping dual vector system. The levels of full-length ABCA4 detected by Western blot in whole *Abca4*$^{-/-}$ eyes treated with dual vector were 1% of the Abca4 levels detected in wild-type eyes. However, such a comparison assumes no loss of photoreceptor cells as a result of injection trauma and retinal detachment and that the injected mice achieve 100% photoreceptor transduction, which is not the case. Despite what may be considered from the Western blots to be relatively low levels of ABCA4 expression across an entire *Abca4*$^{-/-}$ neural retina, the ABCA4 present in eyes treated with dual vector exhibited a detectable reduction in the levels of bisretinoids that accumulate in the mouse model. In patients with Stargardt disease, the bisretinoid accumulation leads to death of the RPE cells and subsequently the photoreceptor cells, which results in blindness. Given the progressive degenerative nature of the disorder, providing therapeutic intervention at any age could be an-

ticipated to be beneficial by preserving the surviving cells of the retina.

This study is a step forward in the difficult task of developing a gene therapy treatment for Stargardt disease and further optimizations of the vector preparation, such as by reducing empty capsid contamination, will be another step toward clinical trial. By optimizing an overlapping dual vector system to increase the levels of therapeutic protein delivered to the target cells and, importantly, reducing the expression of unwanted products that often occur in dual vector strategies, AAV gene therapy clinical trial prospects for Stargardt disease are now looking increasingly achievable.

ACKNOWLEDGMENTS

The project was funded by Medical Research Council DPFS/DCS grant MR/K007629/1 (M.E.M. and R.E.M.) and supported by the National Institute for Health Research Oxford Biomedical Research Centre (A.R.B., M.E.M., and R.E.M.); National Eye Institute grants R01 EY025002 (R.A.R.) and EY000331 Stein Eye Institute Core Grant for Vision Research; Unrestricted Grant from Research to Prevent Blindness, Inc. (New York). Preliminary data were achieved through funding from Fight for Sight UK (R.E.M.).

M.E.M. and R.E.M. designed the project; M.E.M. performed experiments, analyzed the data, and formed the manuscript. A.R.B. and M.S.S. assisted with various technical aspects of the project including subretinal injections. P.C.I. provided preliminary data for the project and imaging expertise; Z.J. and R.A.R. performed HPLC analytical assessments; and R.E.M. obtained funding and supervised the project.

AUTHOR DISCLOSURE

No competing financial interests exist for P.C.I., M.S.S., R.A.R., or Z.J. R.E.M. is the academic founder and a director of Nightstar Therapeutic Inc. (London, UK), a gene therapy company established by the University of Oxford and originally funded by the Wellcome Trust through Syncona Partners. R.E.M. and M.E.M. are named inventors on a patent filed on behalf of the University of Oxford, relating to the optimized *ABCA4* dual vector (PCT/GB2017/051741). R.E.M., A.R.B., and M.E.M. are consultants to Nightstar Therapeutics Inc.

REFERENCES

1. Trapani I, Puppo A, Auricchio A. Vector platforms for gene therapy of inherited retinopathies. Prog Retin Eye Res 2014;43:108–128.
2. Russell S, Bennett J, Wellman JA, et al. Efficacy and safety of voretigene neparvovec (AAV2-hRPE65v2) in patients with RPE65-mediated inherited retinal dystrophy: a randomised, controlled, open-label, phase 3 trial. Lancet 2017;26:849–860.
3. Mingozzi F, High KA. Immune responses to AAV in clinical trials. Curr Gene Ther 2007;7:316–324.
4. MacLaren RE, Groppe M, Barnard AR, et al. Retinal gene therapy in patients with choroideremia: initial findings from a phase 1/2 clinical trial. Lancet 2014;13:62117–62120.
5. Edwards TL, Jolly JK, Groppe M, et al. Visual acuity after retinal gene therapy for choroideremia. N Engl J Med 2016;374:1996–1998.
6. Bennett J, Ashtari M, Wellman J, et al. AAV2 gene therapy readministration in three adults with congenital blindness. Sci Transl Med 2012;4:120–135.
7. Mingozzi F, Maus MV, Hui DJ, et al. CD8(+) T-cell responses to adeno-associated virus capsid in humans. Nat Med 2007;13:419–422.
8. McClements ME, MacLaren RE. Adeno-associated virus (AAV) dual vector strategies for gene therapy encoding large transgenes. Yale J Biol Med 2017; 90: 611–623.
9. Chamberlain K, Riyad JM, Weber T. Expressing transgenes that exceed the packaging capacity of adeno-associated virus capsids. Hum Gene Ther Methods 2016;27:1–12.
10. Dyka FM, Boye SL, Chiodo VA, et al. Dual adeno-associated virus vectors result in efficient in vitro and in vivo expression of an oversized gene, MYO7A. Hum Gene Ther Methods 2014;25:166–177.
11. Carvalho LS, Turunen HT, Wassmer SJ, et al. Evaluating efficiencies of dual AAV approaches for retinal targeting. Front Neurosci 2017;11:1–8.
12. Li J, Sun W, Wang B, et al. Protein trans-splicing as a means for viral vector-mediated in vivo gene therapy. Hum Gene Ther 2008;19:958–964.
13. Allocca M, Doria M, Petrillo M, et al. Serotype-dependent packaging of large genes in adeno-associated viral vectors results in effective gene delivery in mice. J Clin Investig 2008;118:1955–1964.
14. Trapani I, Toriello E, de Simone S, et al. Improved dual AAV vectors with reduced expression of truncated proteins are safe and effective in the retina of a mouse model of Stargardt disease. Hum Mol Genet 2015;24:6811–6825.
15. Colella P, Trapani I, Cesi G, et al. Efficient gene delivery to the cone-enriched pig retina by dual AAV vectors. Gene Ther 2014;21:450–456.
16. Trapani I, Colella P, Sommella A, et al. Effective delivery of large genes to the retina by dual AAV vectors. EMBO Mol Med 2014;6:194–211.
17. McClements ME, Charbel Issa P, Blouin V, et al. A fragmented adeno-associated viral dual vector strategy for treatment of diseases caused by mutations in large genes leads to expression of hybrid transcripts. J Genet Syndr Gene Ther 2016;7:311–319.
18. Stone EM, Andorf SS, DeLuca AP, et al. Clinically focused molecular investigation of 1000 consecutive families with inherited retinal disease. Ophthalmology 2017;124:1314–1331.
19. Tsybovsky Y, Wang B, Quazi F, et al. Post-translational modifications of the photoreceptor-specific ABC transporter ABCA4. Biochemistry 2011;50:6855–6866.
20. Charbel Issa P, Barnard AR, Singh MS, et al. Fundus autofluorescence in the Abca4-/- mouse model of Stargardt disease — correlation with accumulation of A2E, retinal function and histology. Invest Ophthalmol Vis Sci 2013;54:5602–5612.
21. Charbel Issa P, Barnard AR, Herrmann P, et al. Rescue of the Stargardt phenotype in Abca4 knockout mice through inhibition of vitamin A dimerization. Proc Natl Acad Sci U S A 2015;112:8415–8420.
22. Khani SC, Pawlyk BS, Bulgakov OV, et al. AAV-mediated expression targeting of rod and cone

photoreceptors with a human rhodopsin kinase promoter, Invest Ophthalmol Vis Sci 2007;48: 3954–3961.

23. Delori FC, Staurenghi G, Arend O, et al. In vivo measurement of lipofuscin in Stargardt's disease–fundus flavimaculatus. Invest Ophthalmol Vis Sci 1995;36:2327–2331.
24. Radu RA, Yuan Q, Hu J, et al. Accelerated accumulation of lipofuscin pigments in the RPE of a mouse model for ABCA4-mediated retinal dystrophies following vitamin A supplementation. Invest Ophthalmol Vis Sci 2008;49:3821–3829.
25. Petrs-Silva H, Dinculescu H, Li Q, et al. High-efficiency transduction of the mouse retina by tyrosine-mutant AAV serotype vectors. Mol Ther 2009;17:463–471.
26. De Silva SR, Issa PC, Singh MS, et al. Single residue AAV capsid mutation improves transduction of photoreceptors in the Abca4(-/-) mouse and bipolar cells in the rd1 mouse and human retina ex-vivo. Gene Ther 2016;23:767–774.
27. Nott A, Meislin SH, Moore MJ. A quantitative analysis of intron effects on mammalian gene expression. RNA 2003;9:607–617.
28. Flotte TR, Afione SA, Solow R, et al. Expression of the cystic fibrosis transmembrane conductance regulator from a novel adeno-associated virus promoter. J Biol Chem 1993;268:3781–3790.
29. Weng J, Mata NL, Azarian SM, et al. Insights into the function of Rim protein in photoreceptors and etiology of Stargardt's disease from the phenotype in abcr knockout mice. Cell 1999;98:13–23.
30. Charbel Issa P, Singh MS, Lipinski DM, et al. Optimization of in vivo confocal autofluorescence imaging of the ocular fundus in mice and its application to models of human retinal degeneration. Invest Ophthalmol Vis Sci 2012;53:1066–1075.
31. Birtel J, Eisenberger T, Gliem M, et al. Clinical and genetic characteristics of 251 consecutive patients with macular and cone/cone-rod dystrophy. Sci Rep 2018;7:1–11.
32. Beaudoing E, Freier S, Wyatt JR, et al. Patterns of variant polyadenylation signal usage in human genes. Genome Res 2000;10:1001–1010.
33. Tian B, Hu J, Zhang H, et al. A large-scale analysis of mRNA polyadenylation of human and mouse genes. Nucleic Acids Res 2005;33:201–212.
34. Klauer AA, van Hoof A. Degradation of mRNAs that lack a stop codon: a decade of nonstop progress. Wiley interdisciplinary reviews. RNA 2012;3:649–660.
35. Kozak M. Pushing the limits of the scanning mechanism for initiation of translation. Gene 2002;299:1–34.
36. Kozak M. The scanning model for translation: an update. J Cell Biol 1989;108:229–241.
37. Reits, Neijssen J, Herberts C, et al. A major role for TPPII in Trimming proteasomal degradation products for MHC class I antigen presentation. Immunity 2004;20:495–506.
38. Saric T, Graef CI, Goldberg AL. Pathway for degradation of peptides generated by proteasomes: a key role for thimet oligopeptidase and other metallopeptidases. J Biol Chem 2004;279:46723–46732.
39. Proudfoot NJ, Furger A, Dye MJ. Integrating mRNA processing with transcription. Cell 2002; 108:501–512.
40. Han Z, Conley SM, Makkia RS, et al. DNA nanoparticle-mediated ABCA4 delivery rescues Stargardt dystrophy in mice. J Clin Invest 2012;122: 3221–3226.

Received for publication August 3, 2018;
accepted after revision October 30, 2018.

Published online: October 31, 2018.